Fermi Surface Topology of $Ca_{1.5}Sr_{0.5}RuO_4$ Determined by Angle-Resolved Photoelectron Spectroscopy

S.-C. Wang,[1] H.-B. Yang,[1] A. K. P. Sekharan,[1] S. Souma,[2] H. Matsui,[2] T. Sato,[2] T. Takahashi,[2] Chenxi Lu,[3] Jiandi Zhang,[3] R. Jin,[4] D. Mandrus,[4] E. W. Plummer,[4] Z. Wang,[1] and H. Ding[1]

[1]*Department of Physics, Boston College, Chestnut Hill, Massachusetts 02467, USA*
[2]*Department of Physics, Tohoku University, 980-8578 Sendai, Japan*
[3]*Department of Physics, Florida International University, Miami, Florida 33199, USA*
[4]*Condensed Matter Science Division, Oak Ridge National Laboratory, Oak Ridge, Tennessee 37831, USA*
(Received 18 June 2004; published 21 October 2004)

We report angle-resolved photoelectron spectroscopy results of the Fermi surface of $Ca_{1.5}Sr_{0.5}RuO_4$, which is at the boundary of magnetic/orbital instability in the phase diagram of the Ca-substituted Sr ruthenates. Three t_{2g} energy bands and the corresponding Fermi surface sheets are observed, which are also present in the Ca-free Sr_2RuO_4. We find that while the Fermi surface topology of the α, β ($d_{yz,zx}$) sheets remains almost the same in these two materials, the γ (d_{xy}) sheet exhibits a holelike Fermi surface in $Ca_{1.5}Sr_{0.5}RuO_4$ in contrast to being electronlike in Sr_2RuO_4. Our observation of all three volume conserving Fermi surface sheets clearly demonstrates the absence of orbital-selective Mott transition, which was proposed theoretically to explain the unusual transport and magnetic properties in $Ca_{1.5}Sr_{0.5}RuO_4$.

PACS numbers: 74.25.Jb, 72.15.Lh, 74.70.Pq, 79.60.Bm

The discovery of unconventional superconductivity in Sr_2RuO_4 has generated considerable interest in studying the electronic structure of the ruthenates [1]. Sr_2RuO_4, as the only layered perovskite superconductor without copper, has the same crystal structure as the high-T_c cuprate, $La(Sr)_2CuO_4$. As in the case of cuprates, Sr_2RuO_4 can be regarded as being in proximity to a Mott insulator since a complete replacement of Sr by isovalent Ca leads to an antiferromagnetic (AF) insulator state with a moment corresponding to spin $S = 1$ [2]. It is recently discovered that partial substitution of Sr by isoelectronic Ca generates a complex phase diagram for $Ca_{2-x}Sr_xRuO_4$ [3]. At low Sr concentrations ($0 < x < 0.2$), the system is an AF Mott insulator at low temperatures (T); a metal-insulator transition occurs at a higher T. At higher Sr concentrations ($0.2 < x < 0.5$), the system becomes metallic at all T with AF correlations at low T. Upon further increasing Sr ($0.5 < x < 2$), the system becomes a paramagnetic metal, and superconductivity emerges at $x = 2$. The Sr concentration $x_c = 0.5$ is believed to be at a quantum critical point, separating a metallic and orbitally ordered phase ($x < x_c$) from the paramagnetic metal ($x > x_c$) [4]. The spin susceptibility, at the zero temperature limit, is critically enhanced at $x_c = 0.5$, indicating a nearly ferromagnetic instability at this composition [3]. It should be emphasized that since Sr and Ca are isoelectronic, Ca substitution does not change the valence electron numbers in contrast to carrier doping in the cuprate high-T_c superconductors. The rich physical phenomena in this series result rather from the changes in the interplay between electronic correlations and the band structures induced by the crystal structure changes, and the intriguing possibility of ''internal doping'' of selected bands due to the transfer of valence electrons among the orbitals.

The low-energy excitations of $Ca_{2-x}Sr_xRuO_4$ are believed to originate from the hybridization between Ru-4d t_{2g} and O-2p orbitals. It is generally accepted that, at the one end of the phase diagram, Sr_2RuO_4 has four valence electrons evenly distributed in the three t_{2g} orbitals, forming three energy bands α, β (due to the mixing of d_{yz} and d_{zx} states), and γ (d_{xy}). The electron occupancy has the fractions $(n_{(\alpha,\beta)}, n_\gamma) = (\frac{8}{3}, \frac{4}{3})$. At the other end, Ca_2RuO_4's electron distribution is believed to be $(2, 2)$, creating a Mott localized AF ground state at low T [4]. However, the evolution of the electron distribution and band structure in partially substituted $Ca_{2-x}Sr_xRuO_4$ is not fully understood yet. In particular, the knowledge of the electronic structure of $Ca_{1.5}Sr_{0.5}RuO_4$ is important in understanding the alleged critical behavior and the transition to the Mott insulator.

It is proposed by Anisimov *et al.* [4], based on a noncrossing approximation calculation within dynamical mean field theory (DMFT), that the valence electron distribution becomes $(3, 1)$ at x_c. They further proposed that one of the α and β bands hosts two of the three electrons and is thus completely filled and band insulating while the other, half-filled band becomes Mott localized with spin-$\frac{1}{2}$ local moment due to the narrow bandwidth relative to the Coulomb energy (Hubbard U). The half-filled γ band, however, remains itinerant due to its wider bandwidth, resulting in a metallic phase consistent with the experiments [3,5]. This proposal of an apparent orbital-selective Mott transition (OSMT) is of general interest to multiband correlated systems such as transition metal oxides and the heavy fermion compounds. However, the (non)existence of OSMT, particularly in real materials, has been a much debated issue [6–8].

From a quantum mechanical point of view, localized and extended states cannot coexist at the same energy unless quantum tunneling (mixing) between these states is strictly forbidden by symmetry considerations. Indeed, a different quantum Monte Carlo calculation within the DMFT by Liebsch [6] suggests a common metal-insulator transition for all three t_{2g} bands at the same critical correlation U_c. The debate on this issue continues with two recent theoretical papers reaching opposite conclusions [7,8]. However, there has been no experimental test that such OSMT exists in degenerate d-electron systems with small bandwidth difference among orbitals.

Angle-resolved photoelectron spectroscopy (ARPES) is a suitable experimental technique to study this problem because of its ability to determine band dispersion and the Fermi surface in the momentum space. The technique of de Haas–van Alphen (dHvA) is another commonly used method for measuring the Fermi surface. It has played a crucial role in mapping the three Fermi sheets in the undoped Sr_2RuO_4. However, it is difficult to use dHvA to probe Ca-doped ruthenate due to disorder in the doped materials. Therefore ARPES is perhaps a unique experimental tool to resolve this controversy, as suggested originally by Anisimov *et al.* [4]. We have measured extensively $Ca_{1.5}Sr_{0.5}RuO_4$ single crystals and performed a comparative study to Sr_2RuO_4, as reported below.

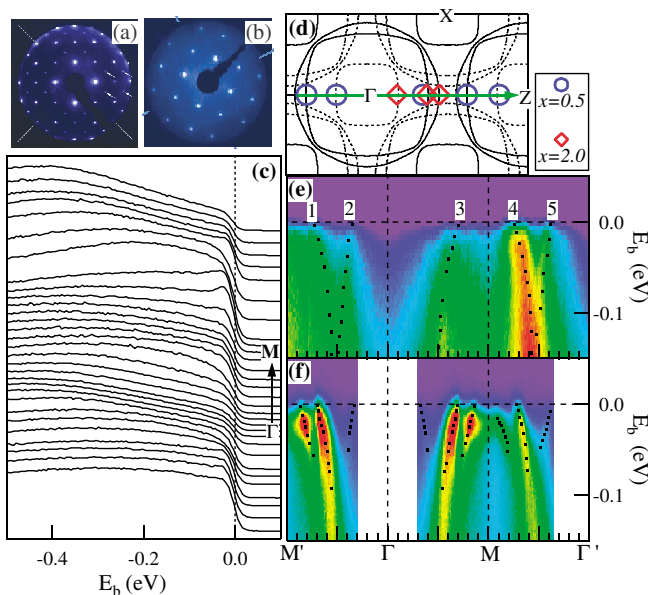High-quality $Ca_{2-x}Sr_xRuO_4$ single crystals are prepared by the floating zone method [9]. ARPES experiments are performed at the Synchrotron Radiation Center, Wisconsin using undulator beam lines (U1 NIM and PGM) at different photon energies (10 to 32 eV). Samples are cleaved *in situ* and measured at $T = 40$ K in a vacuum better than 8×10^{-11} Torr. A Scienta analyzer capable of multiangle detection is used with energy resolution of 10–20 meV, and momentum resolution of ~ 0.02 Å^{-1}. $Ca_{1.5}Sr_{0.5}RuO_4$ are stable and show no sign of degradation during a typical measurement period of 12 h.

Similar to Sr_2RuO_4, $Ca_{1.5}Sr_{0.5}RuO_4$ is easy to cleave and usually has a good (001) surface. Both materials exhibit clear LEED patterns for their cleaved surfaces, as shown in Figs. 1(a) and 1(b). The brighter LEED spots form a square lattice, corresponding to the 2D RuO_2 lattice. The additional faint spots, which appear in the middle of four bright spots, is caused by the rotation of RuO_6 octahedra along the c axis. In Sr_2RuO_4, this rotation is caused by a surface reconstruction driven by a soft phonon mode [10]. However, this rotation is observed to exist in the bulk of $Ca_{2-x}Sr_xRuO_4$ when $x < 1.5$ [11]. For $Ca_{1.5}Sr_{0.5}RuO_4$, the rotation angle in the bulk is about 12° [11]. In comparison, the rotation angle on the surface obtained by LEED analysis is about 11°, indicating similar crystal structures between the bulk and surface. Therefore we expect ARPES results on $Ca_{1.5}Sr_{0.5}RuO_4$ are bulk representative.

Because of the rotation of RuO_6 octahedra, the 2D BZ becomes a $\sqrt{2} \times \sqrt{2}$ lattice rotated 45° with respect to the original 1×1 square lattice. Nevertheless, in this Letter, we still use the 1×1 square lattice to discuss the band structure for convenience in comparison. The main effect of this rotation on the band structure is a band folding with respect to the new zone boundaries. In Sr_2RuO_4, the surface states due to the lattice rotation can be greatly suppressed by varying photon energy or aging the surface in ARPES experiments. Thus bulk-representative band structure and Fermi surface topology, similar to the ones predicted by band calculations [12,13] and observed by dHvA measurement [14], have been observed by ARPES on Sr_2RuO_4 [15–17].

In the following we focus on the electronic structure near E_F, which determines the low-energy properties of this material. In Fig. 1(c) we plot the EDCs of $Ca_{1.5}Sr_{0.5}RuO_4$ along the $(0,0)$-$(\pi,0)$ (Γ-M, the Ru-O bond) direction over several BZs. One can clearly observe band dispersion and Fermi surface crossings (FSCs). To see the dispersion and FSCs more clearly, we display the corresponding E-k intensity plot in Fig. 1(e). We can identify five dispersive bands, as marked in Fig. 1(e). The strongest feature is No. 4 in the second BZ, which has equivalent bands in other BZs, such as No. 1 and No. 3 whose k locations are shifted by a reciprocal lattice vector G. In comparison to band calculations [12,13], dHvA measurements [14], and ARPES results [15–17] on

FIG. 1 (color). LEED patterns for (a) Sr_2RuO_4 and (b) $Ca_{1.5}Sr_{0.5}RuO_4$. (c) Energy distribution curves (EDCs) of $Ca_{1.5}Sr_{0.5}RuO_4$ along Γ-M using 32-eV photons. (d) Measurement locations (green line) in extended Brillouin zones (BZs), with the calculated Fermi surface (FS) (solid lines) of Sr_2RuO_4 and the image FS (dashed lines). FS crossing points are plotted for $Ca_{1.5}Sr_{0.5}RuO_4$ (blue circles) and Sr_2RuO_4 (red diamonds) extracted from panels below. E-k intensity plots for (e) $Ca_{1.5}Sr_{0.5}RuO_4$, and (f) Sr_2RuO_4. The dots are guides for band dispersion.

Sr_2RuO_4, we find that these bands (No. 1, No. 3, and No. 4) match almost perfectly to the β band. As an illustration, we plot the extracted FSCs of $Ca_{1.5}Sr_{0.5}RuO_4$ in Fig. 1(d) where the calculated Sr_2RuO_4 FS sheets (solid lines) are shown. In Fig. 1(d) we also plot the FSCs of Sr_2RuO_4 extracted from Fig. 1(f).

Figure 1(f) displays an E-k intensity plot along Γ-M for Sr_2RuO_4. In addition to the β band, the γ band is observed near M. However, no such a band is visible along Γ-M in $Ca_{1.5}Sr_{0.5}RuO_4$, as shown in Fig. 1(e). One may argue that the observed bands (No. 1, No. 3, and No. 4) belong to the γ band that shrinks its FS area upon Ca substitution. This scenario is unlikely due to the observation of a reversed band dispersion, such as No. 5 and No. 2 in Fig. 1(e). We attribute this reversed band dispersion to a folded α band caused by the rotation of RuO_6 octahedra in the bulk of $Ca_{1.5}Sr_{0.5}RuO_4$ [11]. This band folding introduces the so-called "image" FS, as shown in Fig. 1(d) (dashed lines). The FSCs of the reversed bands No. 5 and No. 2 match well with the predicted image of α FS. Note a similar band folding is also observed in Sr_2RuO_4, which is due to the rotation of RuO_6 octahedra on the surface, as discussed before.

As seen in the band calculation, the three Fermi surfaces are adjacent in the vicinity of $(2/3\pi, 2/3\pi)$. Thus this location is a good place to observe all the three FS and their relative positions. This is clearly demonstrated in the case of Sr_2RuO_4, as shown in Fig. 2(a), where the near-E_F (± 20 meV) intensity is plotted in a 2D k region indicated by the shaded rectangular area (I) in the BZ shown in Fig. 2(c). One can clearly observe the three (α, β, γ) FS sheets in Fig. 2(a), although the intensity of the β FS is much weaker along Γ-X. This is most likely due to the selection rule of ARPES. While the α and β FS sheets are well separated due to orbital hybridization between them, the γ FS "touches" the α FS along Γ-X, reflecting the nonmixing nature between the xy and $yz(zx)$ orbitals, as predicted based on a symmetry argument [18]. In addition, we observe the folded γ' FS and a
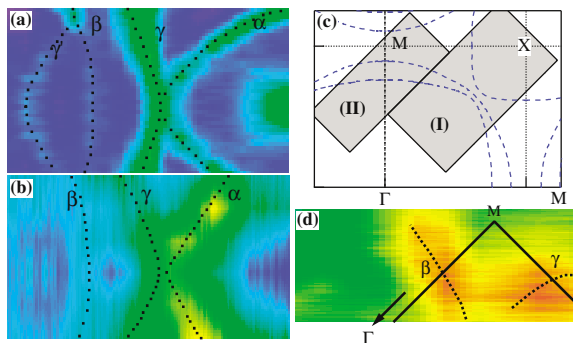
small FS pocket at the X point, which is believed to be the result of the rotation of RuO_6 octahedra on the surface of Sr_2RuO_4 [17].

For $Ca_{1.5}Sr_{0.5}RuO_4$, as shown in Fig. 2(b), one can still observe the three FS sheets, although their intensity is weaker than in Sr_2RuO_4. The reduction in spectral intensity at E_F is commonly observed in doped correlated systems. This decoherence phenomenon is believed to be caused by correlation and disorder effects. Among the three FSs, the α FS is the most visible. A "faint" FS, which touches the α FS along Γ-X, should belong to the γ band due to its nonmixing or weak mixing with the α band. Another less visible FS, which is further separated from the α FS, is naturally assigned to the β band.

As discussed above, we do not observe the γ FS crossing along Γ-M. It is possible that the γ FS changes its topology from electronlike centered at Γ to holelike centered at X. To check this, we measured the ARPES spectra in the vicinity of M, indicated by the rectangular box (II) in the BZ shown in Fig. 2(c). From the plot of the near-E_F intensity in Fig. 2(d), one can observe two FS sections: the one intersecting with Γ-M belongs to the β FS, and the other intersecting with M-Y should be the γ FS which becomes holelike by enclosing the X point.

We summarize our ARPES results of $Ca_{1.5}Sr_{0.5}RuO_4$ by plotting its measured Fermi surface in Fig. 3. The blue circles are the FS crossing points directly obtained from ARPES spectra. The black solid lines are derived Fermi surfaces based on the measurement and trivial symmetry operations. For the purpose of comparison, we also plot in Fig. 3 the Fermi surfaces (red dashed lines) of Sr_2RuO_4 determined from our ARPES experiment. It is clear from Fig. 3 that all the three FS sheets, with similar topology, are observed in both $Ca_{1.5}Sr_{0.5}RuO_4$ and Sr_2RuO_4 with the significant difference that the γ FS changes from electronlike in Sr_2RuO_4 to holelike in $Ca_{1.5}Sr_{0.5}RuO_4$. This change is consistent with the local-density approxi-

FIG. 2 (color). 2D plots of intensity integrated over a small energy region of E_F (± 20 meV) for (a) Sr_2RuO_4 in the rectangular box (I) shown in (c); (b) $Ca_{1.5}Sr_{0.5}RuO_4$ in the same box (I); (d) $Ca_{1.5}Sr_{0.5}RuO_4$ in the box (II). (c) Locations of measurement in the BZ.
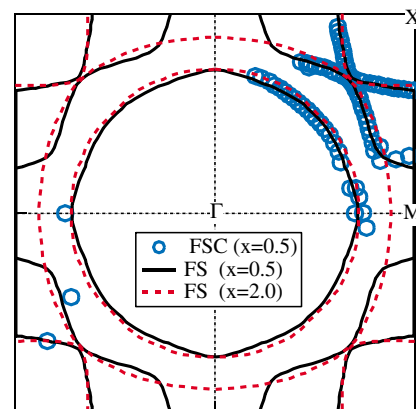

FIG. 3 (color). Measured FS crossing points (blue circles) and derived Fermi surfaces (solid black lines) in $Ca_{1.5}Sr_{0.5}RuO_4$. For comparison, extracted FSs (red dashed lines) in Sr_2RuO_4 are also plotted . Note the folded image FSs are not plotted for clarity.

TABLE I. k_F of FS crossing points along high symmetry lines, and the occupied FS area in $Ca_{1.5}Sr_{0.5}RuO_4$ and Sr_2RuO_4. The experimental uncertainty of k_F is ± 0.04. The unit of k_F is π/a, where $a = 3.76$ (3.86) Å for $Ca_{1.5}Sr_{0.5}RuO_4$ (Sr_2RuO_4).

	$Ca_{1.5}Sr_{0.5}RuO_4$	Sr_2RuO_4
$k_F(x)$ (Γ-M)	$\beta(0.72)$	$\beta(0.72)$, $\gamma(0.88)$
$k_F(x = y)$ (Γ-X)	$\alpha/\gamma(0.67)$, $\beta(0.50)$	$\alpha/\gamma(0.67)$, $\beta(0.51)$
$k_F(y)$ (M-X)	$\alpha(0.62)$, $\gamma(0.22)$	$\alpha(0.64)$
FS area	$\alpha(0.86)$, $\beta(0.38)$, $\gamma(0.68)$	$\alpha(0.86)$, $\beta(0.41)$, $\gamma(0.64)$
Total area	1.92	1.91

mation band calculations [13,19,20] for the rotated crystal structure. A similar change of the γ FS topology is also observed for the surface state in Sr_2RuO_4, which has the similar structure rotation on the surface [17].

From the determined FS topology in Fig. 3, we can extract the values of the Fermi vector (k_F) for the three Fermi surface sheets along the high symmetry lines, as listed in Table I. We note that the k_F values are similar to the ones obtained from the dHvA measurement [14] for Sr_2RuO_4. We also determined the occupied area for the three FS sheets and find no appreciable differences between the two materials. These observations suggest that there is no significant electron transfer among the three orbitals at this Ca doping level, in contrast to the scenario proposed by Anisimov *et al.* [4]. The total occupied areas of the two materials are close to 2, indicative of four electrons per unit cell, satisfying Luttinger theorem.

The observation of all three Fermi surface sheets in $Ca_{1.5}Sr_{0.5}RuO_4$ and the lack of significant interorbital electron transfer clearly demonstrate the absence of OSMT in this material. The proposal of OSMT at $x = 0.5$ was originally motivated by the experimental observation of spin-$\frac{1}{2}$ local moment [4]. The evidence for the $\frac{1}{2}$ local moment comes from fitting the magnetic susceptibility in $Ca_{1.5}Sr_{0.5}RuO_4$ with the Curie-Weiss form. Our observation of three itinerant orbitals appears to be inconsistent with the existence of such localized moments, although more exotic mechanisms may account for (to a certain degree) the coexistence of the local moment and itinerant electrons. We note a recent polarized neutron diffraction experiment for $x = 0.5$ [21] suggesting that the dominant magnetization distribution originates from the xy orbital rather than the yz/zx orbitals predicted by the OSMT theory. Nevertheless, the question of what type of Mott transition takes place upon further Ca doping remains. Whether or not it goes through OSMT is still an open issue and requires more experimental efforts. A recent high-field study [22] reports the saturation magnetic moment in $Ca_{1.8}Sr_{0.5}RuO_4$ ($x = 0.2$) is close to the effective magneton of $1\mu_B$ that is expected from a system with a local moment of $S = 1/2$, indicating a possible OSMT at $x = 0.2$.

In summary, we observe all three t_{2g} bands and the corresponding Fermi surface sheets in both $Ca_{1.5}Sr_{0.5}RuO_4$ and Sr_2RuO_4 by ARPES experiment. The most significant change of the Fermi surface topology is the γ Fermi surface which becomes holelike in $Ca_{1.5}Sr_{0.5}RuO_4$ near the M point, while being electronlike in Sr_2RuO_4. This is likely caused by the rotation of RuO_6 octahedra along the c axis in the bulk upon the Ca substitution. Together with our observation that the electron filling fractions are conserved approximately within each of the t_{2g} orbitals when compared to Sr_2RuO_4, we conclude that the orbital-selective Mott transition is absent at $x = 0.5$ and call for further understanding of the electronic structure, correlation effects, transport, and magnetic properties in Ca-doped ruthenates.

[1] Y. Maeno *et al.*, Nature (London) **372**, 532 (1994).
[2] G. Cao *et al.*, Phys. Rev. B **56**, R2916 (1997).
[3] S. Nakatsuji and Y. Maeno, Phys. Rev. Lett. **84**, 2666 (2000).
[4] V. I. Anisimov *et al.*, Eur. Phys. J. B **25**, 191 (2002).
[5] S. Nakatsuji and Y. Maeno, Phys. Rev. B **62**, 6458 (2000).
[6] A. Liebsch, Europhys. Lett. **63**, 97 (2003); Phys. Rev. Lett. **91**, 226401 (2003).
[7] A. Koga *et al.*, cond-mat/0401223.
[8] A. Liebsch, cond-mat/0405410.
[9] R. Jin *et al.*, cond-mat/0112405.
[10] R. Matzdorf *et al.*, Science **289**, 746 (2000).
[11] O. Friedt *et al.*, Phys. Rev. B **63**, 174432 (2001).
[12] T. Oguchi *et al.*, Phys. Rev. B **51**, 1385 (1995).
[13] D. J. Singh *et al.*, Phys. Rev. B **52**, 13 358 (1995).
[14] A. P. Mackenzie *et al.*, Phys. Rev. Lett. **76**, 3786 (1996).
[15] A. Damascelli *et al.*, Phys. Rev. Lett. **85**, 5194 (2000).
[16] H. Ding *et al.*, Physica (Amsterdam) **364C**, 594 (2001).
[17] K. M. Shen *et al.*, Phys. Rev. B **64**, 180502 (2001).
[18] D. F. Agterberg, T. M. Rice, and M. Sigrist, Phys. Rev. Lett. **78**, 3374 (1997).
[19] Z. Fang and K. Terakura, Phys. Rev. B **64**, 020509 (2001).
[20] Z. Fang, N. Nagaosa, and K. Terakura, Phys. Rev. B **69**, 045116 (2004).
[21] A. Gukasov *et al.*, Phys. Rev. Lett. **89**, 87202 (2002).
[22] S. Nakatsuji *et al.*, Phys. Rev. Lett. **90**, 137202 (2003).